Chemie der Erde xxx (xxxx) xxx–xxx

Contents lists available at ScienceDirect

Chemie der Erde

journal homepage: www.elsevier.com/locate/chemer

Petrogenesis and geochronology of Mishao peraluminous I-type granites, Shalair valley area, NE Iraq

Imad Kadhim Abdulzahra[a,*], Ayten Hadi[b], Yoshihiro Asahara[c], Hossein Azizi[d], Koshi Yamamoto[c]

[a] Iraq Geological Survey, Al-Andalus Square, Baghdad, Iraq
[b] Department of Geology, College of Science, University of Baghdad, Baghdad, Iraq
[c] Department of Earth and Environmental Sciences, Graduate School of Environmental Studies, Nagoya University, Nagoya, 464-8601, Japan
[d] Mining Department, Faculty of Engineering, University of Kurdistan, Sanandaj, Iran

ARTICLE INFO

Keywords:
Middle cretaceous granite
Zircon U-Pb age
Sr-Nd isotopes
Neo-Tethys
Iraq

ABSTRACT

The Shalair area, which is located in northeastern Iraq, is considered to be part of the northern Sanandaj-Sirjan Zone (SaSZ) and contains several granitoid bodies. One of these bodies, the Mishao porphyritic-granite (MG), was crystallized at 111.6 ± 2.4 Ma, based on its zircon U-Pb age. Its geochemical characteristics suggest that the MG rocks are calc-alkaline, peraluminous, I-type granites with micrогranular mafic enclaves. They are enriched in SiO_2, Na_2O, Al_2O_3 and Zr and depleted in MgO, Fe_2O_3, Nb and Ti; in contrast, the enclave sample records lower SiO_2 content and higher contents of MgO and Fe_2O_3. These rocks show an enrichment of LREE relative to HREE, and pronounced negative Eu anomalies implying feldspar fractionation. The isotopic and geochemical characteristics of the MG samples suggest that these rocks are evolved through fractional crystallization. In the La/Nb-Nb diagram and Sm/Nd ratios, the MG rocks and the enclave samples exhibit strong evidence for crustal contamination. The MG rocks record high initial $^{87}Sr/^{86}Sr$ (0.70625–0.70740) and low $^{143}Nd/^{144}Nd(i)$ (0.51235–0.51274) ratios. These Sr-Nd isotopic data, combined with the presence of high Th/U and Rb/Sr ratios and significant depletions of Nb, Ta and Ti, show a relation of these bodies to an active continental margin regime. Based on the age and geochemical data of the MG, this study presents new information about the occurrence of Middle Cretaceous magmatic activities, which are related to the active continental margins in the SaSZ that run parallel to the Zagros Fold-Thrust Belt.

1. Introduction

Iraq is located in the northeastern margin of the Arabian Platform, which is located within the Zagros Orogenic Belt. The formation of the Zagros Orogenic Belt has been attributed to the long-lasting convergence of (and the interactions between) Eurasia and Gondwana (Alavi, 1980,1994; Berberian and King, 1981). The geodynamic evolution of the Zagros Belt is mainly related to the opening and closure of the Neo-Tethys Ocean (Alavi, 1994; Allahyari et al., 2010; Chiu et al., 2013). The Sanandaj-Sirjan Zone (SaSZ) is an active margin of the Central Iranian Block, which has produced calc-alkaline magmatic activity (e.g., Ahmadi Khalaji et al., 2007; Berberian and King, 1981; Dewey et al., 1973; Haynes and McQuillan, 1974; Ghasemi and Talbot, 2006; Sengor, 1990; Fazlnia et al., 2009). This magmatic activity was shifted progressively northward during the Mesozoic (Agard et al., 2005). The SaSZ is characterized by metamorphic rocks that have been deformed multiple times, as well as Mesozoic volcanic rocks and an abundance of multiply deformed and undeformed plutonic assemblages (Mohajjel et al., 2003; Azizi and Jahangiri, 2008). The ages of the SaSZ plutons range from Neoproterozoic (Hassanzadeh et al., 2008; Shafaii Moghadam et al., 2017), Paleozoic (e.g., Abdulzahra et al., 2016; Alirezaei and Hassanzadeh, 2012; Bea et al., 2011; Shakerardakani et al., 2015), and Mesozoic (e.g., Ahmadi Khalaji et al., 2007; Azizi et al., 2011a, 2015; Chiu et al., 2013; Esna-Ashari et al., 2012; Fazlnia et al., 2009; Mahmoudi et al., 2011; Shahbazi et al., 2010) to Tertiary (e.g., Ahmadi Khalaji et al., 2007; Azizi et al., 2011b, 2015; Fazlnia et al., 2009; Mazhari et al., 2009). Few studies of the Cretaceous granitoids in the SaSZ have used zircon U-Pb dating to analyze the subduction-related magmatism of the Neo-Tethys Ocean in an active continental margin regime within the southwestern region of the SaSZ (Abdulzahra et al., 2017; Mahmoudi et al., 2011; Mazhari et al., 2011; this study). However, Agard et al. (2011) suggested that the Middle to Late Cretaceous period (115–85 Ma) was marked by the perturbation of subduction associated with blue schist-facies exhumation along the northern edge of the Neo-Tethys subduction zone with the development of a supra-subduction zone ophiolite during the Late Cretaceous. The

* Corresponding author.
E-mail address: emadalsaffi@yahoo.com (I.K. Abdulzahra).

https://doi.org/10.1016/j.chemer.2018.01.003
Received 9 September 2017; Received in revised form 27 December 2017; Accepted 24 January 2018
0009-2819/

Please cite this article as: Abdulzahra, I.K., Chemie der Erde (2018), https://doi.org/10.1016/j.chemer.2018.01.003

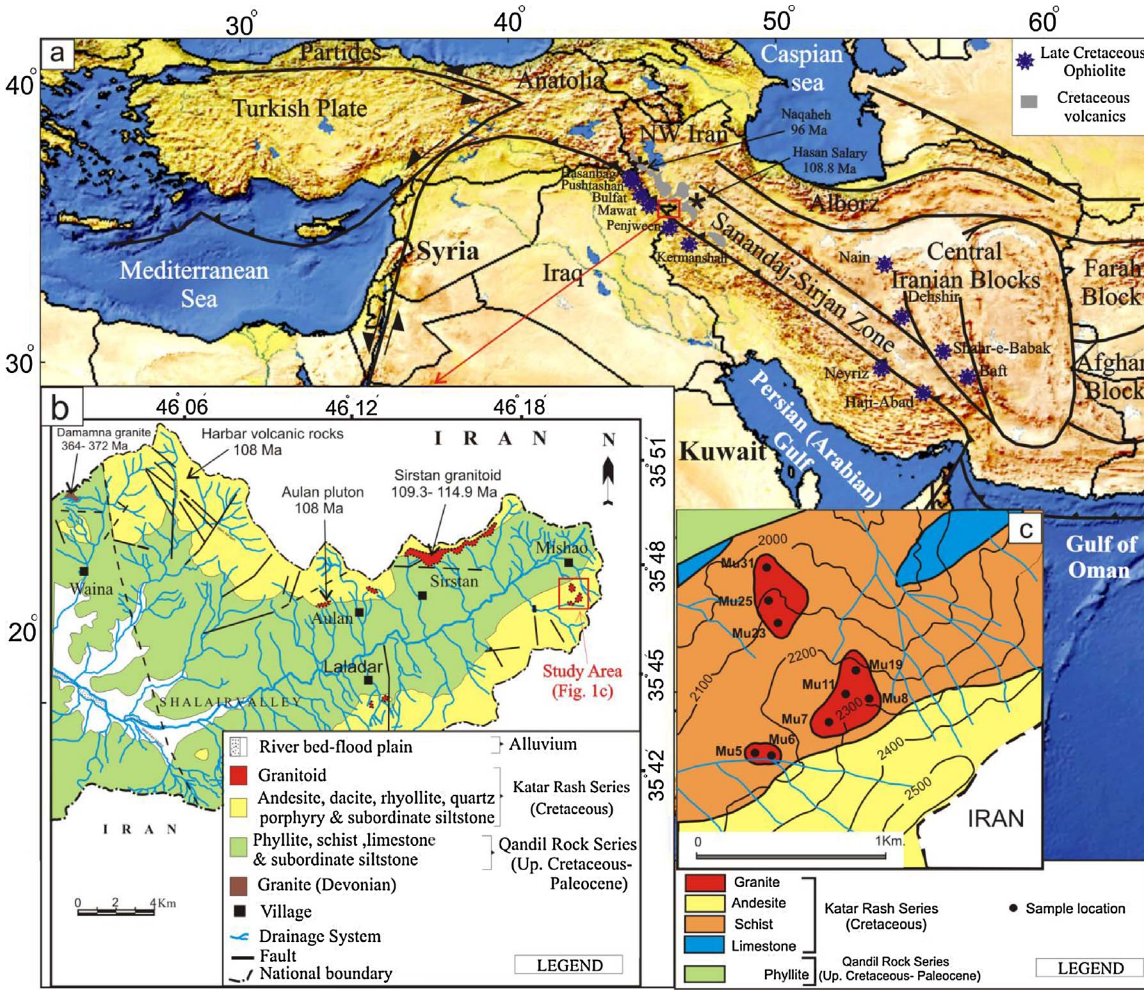

Fig. 1. (a) Location map of the study area (made with Natural Earth; free vector and raster map data available at naturalearthdata.com). (b) Geological map of the Shalair Valley area modified from Al-Shible and Kettaneh (1972). (c) Sample locations of the Mishao granites (MG) are shown as solid circles (after Al-Shible and Kettaneh, 1972). Data sources of zircon U-Pb ages are from Abdulzahra et al. (2016, 2017), Ali et al. (2016), Mahmoudi et al. (2011) and Mazhari et al. (2011). Note that the age of the MG has been considerably revised in this study (i.e., Albian).

SaSZ is separated into inner and outer ophiolite belts, which have supra-subduction zone affinities (Shafaii Moghadam and Stern, 2011). The inner and outer ophiolite belts are mainly composed of mantle and crustal sequences ranging from mantle harzburgite to crustal lavas (Shafaii Moghadam and Stern, 2011). In northeastern Iraq, dismembered ophiolites have been documented at Hasanbag, Pushtashan, Bulfat, Mawat and Penjween (Fig. 1a); some of them, such as Penjween, show good correlations with the outer ophiolite belt in Iran (Ali et al., 2012). Further details on the geology of ophiolites in Iraq have been provided by Jassim and Goff (2006).

The Misho granites (MG) that are situated in the Shalair Valley area within the Iraqi Zagros Suture Zone in the border of Iran and Iraq has not been studied in detail because of many problems in the last three decades. The present study reports new zircon U-Pb age, as well as chemical and Sr-Nd isotopic data. These data have been used to better understand the petrogenesis, geochronology and tectono-magmatic evolution of northern Arabia and northwestern Iran during the Middle Cretaceous.

2. Geological setting and field observations

The Iraqi Suture Zone is a narrow tectonic zone, formed within the Neo-Tethys Ocean and then was thrusted over the Arabian Plate by obduction during the Late Cretaceous, which was followed by collision during the Miocene-Pliocene (Ali et al., 2012, 2013, 2016; Buday and Jassim, 1987; Jassim and Goff, 2006). The Suture Zone comprises three major units: the Qulqula–Khwakurk, Penjween–Walash and Shalair units (Buday and Jassim, 1987; Jassim and Goff, 2006). The Shalair unit (which is also called the Shalair Terrane; Fouad, 2014, 2015) is located within the Sanandaj-Sirjan Zone (SaSZ), which runs parallel to the Zagros Fold-Thrust Belt. This zone is believed to represent the highest thrust sheet and is located in the Shalair Valley area, which is located in the northeastern most region of Iraq (Fig. 1b). The SaSZ in Iraq and Iran spans a narrow range that is approximately 1500 km long and 150–250 km wide; the major sections of the SaSZ are located in Iran (Alavi, 2004; Allahyari et al., 2010; Mohajjel et al., 2003). The study area is located in the Shalair Valley and comprises an asymmetrical east-west-trending anticline that gently plunges toward the east (Al-Shible and Kettaneh, 1972; Smirnov and Nelidov, 1962) (Fig. 1b). The core of this anticline is covered by the Qandile rock series, which comprises 2000 m of phyllite, schist, slate and greywacke (Buday, 1980; De Villiers, 1957). The Katar Rash volcanic series is exposed along the limbs of the Shalair anticline and comprises approximately 1000 m of calc-alkaline andesite rock with basaltic andesite, dacite and rhyolite (Jassim and Goff, 2006). The age of these volcanic rocks has been reported to be 108 Ma, based on the U-Pb dating of zircon (Ali et al., 2016).

Four intrusive granitic bodies crop out along the limbs of the Shalair anticline within the Katar Rash volcanic series and are represented by the Aulan, Sirstan, Laladar and Mishao granites (Fig. 1b). The ages of

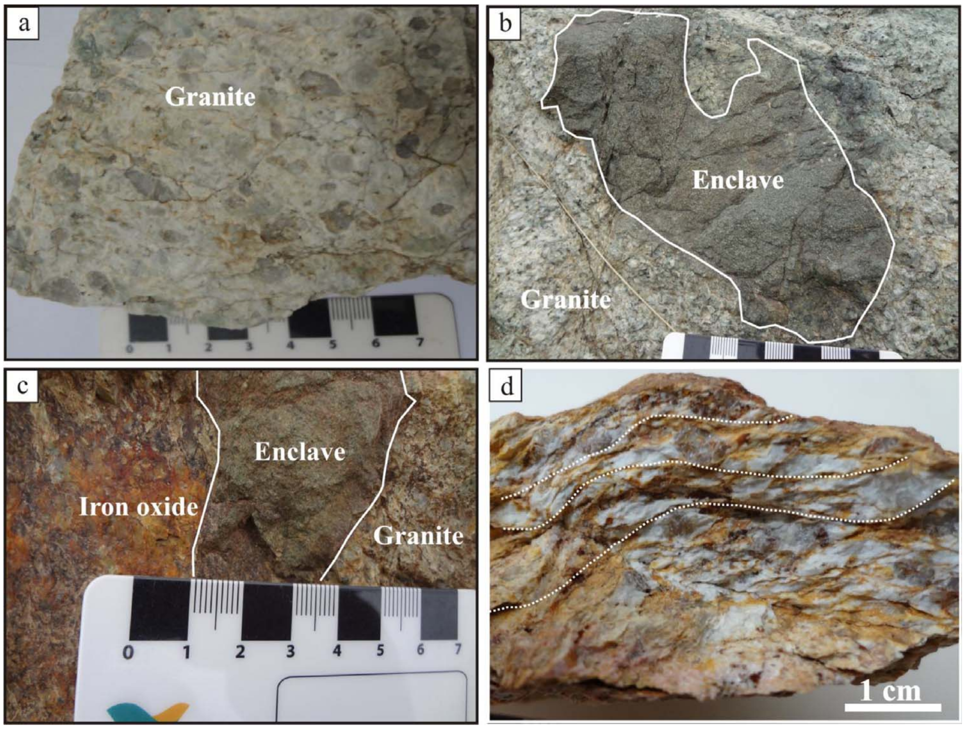

Fig. 2. (a, b) Coarse-grained granites with mafic enclaves in the MG body. (c) Iron oxide enrichment. (d) Sorting of banding minerals in the MG rocks.

these granitoid rocks, based on their U-Pb zircon ages, are 108 Ma for the Aulan rocks (Ali et al., 2016) and 110 Ma for the Sirstan granitoid rocks (Abdulzahra et al., 2017). One intrusive body (the Dammana body) crops out within the Qandil Rock series in the core of this anticline and records zircon U-Pb ages ranging from 364 to 372 Ma (Fig. 1b) (Abdulzahra et al., 2016). In this study, we focus on the Mishao granitic rocks (MG) in order to evaluate the relationship between their ages with those of other bodies that are exposed in the limbs of the Shalair anticline, as well as their tectonic and genetic relationships.

The Mishao granitic rocks (MG) comprise three bodies that are located to the south of Mishao village (Fig. 1b). All of these rocks are exposed at the southern lib of the Shalair anticline within the Katar-Rash volcanic rocks and are surrounded by schist (Fig. 1b, c). The MG rocks are coarse-grained, porphyritic and contain numerous enclaves (Fig. 2a–c) (Abdulzahra and Hadi, 2017). In some areas, they exhibit banding, especially where they are in contact with schist (Fig. 2d). Quartz veins have formed and cut across these rocks; in some areas, iron oxides are observed (Fig. 2c).

3. Analytical techniques

Following the examination of thin sections, nine representative samples and one enclave sample were chosen for the analysis of their chemical compositions and Sr-Nd isotopic ratios. The compositions of major elements were determined using WD-XRF (Rigaku ZSX Primus II) at Nagoya University, Japan. A glass bead comprising a mixture of 0.5 g of sample plus 5.0 g of lithium tetraborate was prepared for XRF analysis. The GSJ reference rocks of JA-1, JA-2, JG-1a, JG-2 and JG-3 were also measured together with the samples. To measure L.O.I. and H_2O–, 0.4 g of rock powder from each sample was placed into a pre-weighted quartz crucible and dried in a drying oven for 12 h at 110 °C (H_2O–); then, the samples were heated in a furnace for 3 h at 900 °C (L.O.I.). The values of H_2O− and L.O.I. (in weight percent) were calculated for each sample based on the difference in the mass recorded before and after heating.

To analyze the Sr and Nd isotopic compositions and trace element concentrations of each sample, 100 mg of each powdered sample was decomposed in HF + $HClO_4$ in two steps to assure its complete decomposition (see Abdulzahra et al., 2016 for details). The decomposed sample was then dissolved in HCl and split into two aliquots in proportions of 1.5:8.5. The former portion was used for the quantitative analysis of trace elements, including REE; the latter portion was used for the analysis of the natural isotopes of Sr and Nd. To isolate Sr and REEs, including Nd, conventional column chemistry was carried out, using cation exchange resin (BioRad AG50W-X8, 200–400 mesh) with an eluent of HCl. To separate Nd from the extracted REE, the cation exchange column was used with an eluent of α-hydroxyisobutyric acid (α-HIBA). Strontium and Nd isotopic compositions were measured using thermal ionization mass spectrometry (TIMS), using the VG Sector 54–30 and GVI IsoProbe-T, respectively, at Nagoya University, Japan. The mass fractionation during Sr-Nd isotopic measurements was corrected based on the accepted values of $^{86}Sr/^{88}Sr = 0.1194$ and $^{146}Nd/^{144}Nd = 0.7219$. In this study, the NIST-SRM 987 and JNdi-1 standards (Tanaka et al., 2000) were also measured for their natural isotopic ratios of Sr and Nd, respectively. More detailed descriptions of these quantitative and isotopic analyses are provided by Azizi and Asahara (2013) and Abdulzahra et al. (2016).

To measure U-Pb ages in zircon, zircon grains were separated from one sample of the Mishao bodies in order to determine their magmatic age. This was carried out using the conventional techniques of heavy liquid and magnetic separation. Cathodoluminescence images (CL) were obtained using scanning electron microscopy (SEM) (Hitachi S-3400N) in order to study the internal structures of zircons and to locate ideal sites for analysis. Zircon U-Pb analyses were performed using an inductively coupled plasma-mass spectrometer (ICP-MS, Agilent 7700x) that was connected to a laser ablation system (LA), NWR213 (Electro Scientific Industries, USA), at Nagoya University, Japan. For U-Pb analyses, the NIST SRM 610 glass standard (Goolaerts et al., 2004) was calibrated using the 91500 zircon standard. A detailed description of the LA-ICP-MS analytical method is provided by Kouchi et al. (2015) and Orihashi et al. (2008). The age of the MG was calculated using the ISOPLOT v. 4.15 software (Ludwig, 2012).

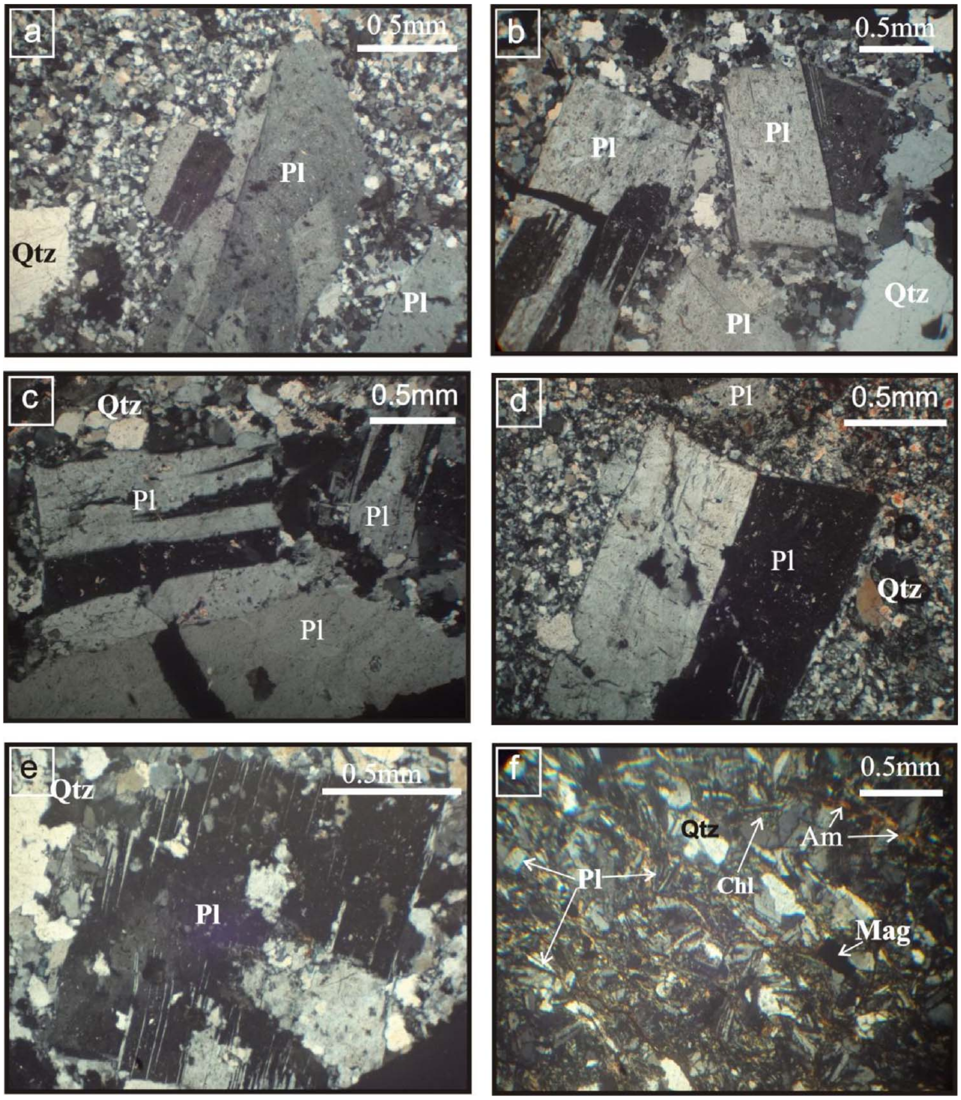

Fig. 3. Photomicrographs of the MG body. (a, b) Porphyritic texture, samples Mu8 and Mu 7 respectively. (c, d, e) Deformation, fracturing and granulation of plagioclase, samples Mu6, Mu11 and Mu5 respectively. (f) Mineralogy of enclave sample XeMu, showing similar mineral compositions as the MG host rocks. Symbols: Pl = plagioclase; Qtz = quartz; Mag = magnetite; Am = amphibole; Chl = chlorite.

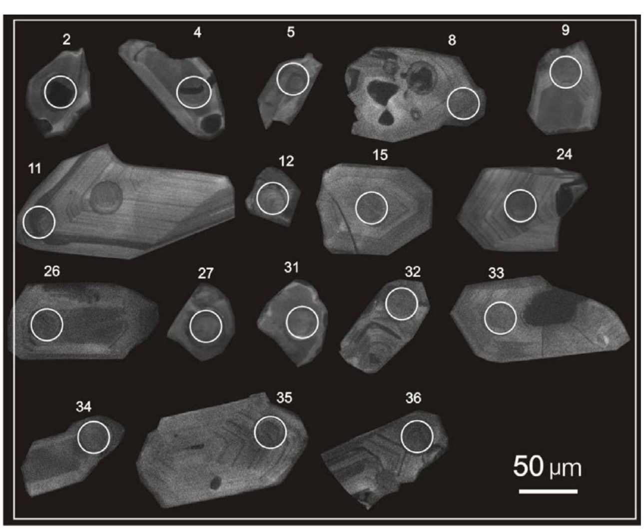

Fig. 4. Cathodoluminescence images (CL) of zircon grains from the MG rocks.

4. Results

4.1. Petrography

The petrographic analysis of the three MG bodies shows that all three bodies are porphyritic (Fig. 3a, b). The mineralogic compositions of the southwestern and southeastern bodies of the MG are identical; plagioclase (35%) and quartz (22%) are the main phenocrysts, with groundmass comprising approximately 43% of the samples. The northern body has a higher groundmass content, reaching a maximum value of 75%, with quartz (15%) and plagioclase (10%) as its main phenocrysts (Abdulzahra and Hadi, 2017). Hornblende and rare pyroxene, as well as zircon and iron oxides, are the main accessory mineral phases, which form as both phenocrysts and groundmass. The compositions of the plagioclase crystals range from oligoclase to andesine. These crystals are anhedral to subhedral, with an average grain size of approximately 1.5 mm. In some of the studied samples, the plagioclase crystals display evidence of deformation, fracturing and granulation (Fig. 3c–e). Quartz crystals are anhedral to subhedral, with an average grain size of approximately 1.8 mm. Some quartz grains exhibit wavy extinction due to deformation. The groundmass mainly comprises fine grains of plagioclase and quartz with minor amounts of accessory minerals, including zircon, pyroxene, amphibole and iron oxides. Chlorite and sericite are rarely observed in the groundmass as the alteration products of both mafic minerals and plagioclase (Abdulzahra and Hadi,

Table 1
LA-ICP-MS analyses for zircon grains from the Mishao granites (Mu11).

Spot	Th/U	^{206}Pbc* (%)	^{207}Pb/^{206}Pb	± Error 2σ	^{206}Pb/^{238}U	± Error 2σ	^{207}Pb/^{235}U	± Error 2σ	^{238}U/^{206}Pb age (Ma)	± Error 2σ	^{235}U/^{207}Pb age (Ma)	± Error 2σ
Mu11												
Mu11-2	0.66	1.09	0.0484	0.0063	0.01813	0.00075	0.1211	0.0166	115.8	4.8	116.1	15.9
Mu11-4	0.65	0.00	0.0502	0.0045	0.01820	0.00066	0.1261	0.0122	116.3	4.2	120.6	11.7
Mu11-5	0.89	0.00	0.0518	0.0050	0.01642	0.00061	0.1173	0.0122	105.0	3.9	112.7	11.7
Mu11-6	1.04	0.00	0.0538	0.0078	0.01623	0.00072	0.1203	0.0183	103.8	4.6	115.3	17.5
Mu11-8	0.69	0.00	0.0474	0.0066	0.01723	0.00073	0.1125	0.0165	110.1	4.7	108.2	15.9
Mu11-9	0.55	0.00	0.0540	0.0084	0.01820	0.00084	0.1355	0.0221	116.2	5.4	129.0	21.0
Mu11-11	0.73	0.25	0.0497	0.0040	0.01771	0.00052	0.1214	0.0104	113.1	3.3	116.3	10.0
Mu11-12	0.62	0.00	0.0467	0.0060	0.01874	0.00067	0.1206	0.0160	119.7	4.3	115.6	15.4
Mu11-15	0.60	0.43	0.0537	0.0073	0.01852	0.00072	0.1372	0.0193	118.3	4.6	130.5	18.4
Mu11-23	0.82	5.51	0.0553	0.0067	0.01616	0.00061	0.1233	0.0157	103.4	3.9	118.1	15.0
Mu11-24	0.53	0.48	0.0473	0.0074	0.01760	0.00074	0.1149	0.0187	112.4	4.7	110.4	18.0
Mu11-26	0.55	0.00	0.0472	0.0068	0.01782	0.00071	0.1160	0.0172	113.8	4.5	111.5	16.5
Mu11-27	0.85	2.20	0.0521	0.0052	0.01696	0.00058	0.1219	0.0128	108.4	3.7	116.8	12.2
Mu11-31	0.58	0.00	0.0553	0.0084	0.01803	0.00080	0.1374	0.0216	115.2	5.1	130.7	20.6
Mu11-32	0.57	0.00	0.0478	0.0074	0.01816	0.00078	0.1197	0.0192	116.0	5.0	114.8	18.4
Mu11-33	0.57	0.00	0.0532	0.0077	0.01788	0.00076	0.1311	0.0198	114.2	4.9	125.1	18.9
Mu11-34	0.47	0.00	0.0476	0.0073	0.01664	0.00071	0.1091	0.0173	106.4	4.5	105.1	16.7
Mu11-35	0.58	0.00	0.0494	0.0069	0.01731	0.00071	0.1178	0.0171	110.6	4.5	113.1	16.4
Mu11-36	0.59	0.00	0.0491	0.0075	0.01701	0.00073	0.1152	0.0182	108.7	4.7	110.7	17.5

^{206}Pb$_c$ is percentage of contributed by common Pb on the basis of ^{204}Pb signal. Value of common Pb was assumed by Stacey and Kramers (1975).

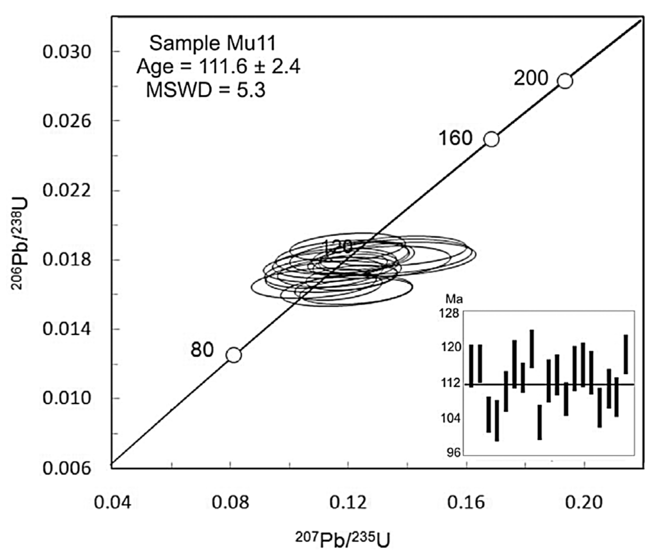

Fig. 5. U-Pb concordia age for the MG rocks. Data-point error ellipses are 2σ.

2017) (Fig. 3f).

The enclave sample (XeMu) exhibits a roughly similar mineralogical composition as the enclosing host granitoids, but is finer-grained and contains more mafic minerals, which are mainly amphibole, pyroxene and chlorite. These mafic minerals are surrounded by quartz and plagioclase, thus forming a microgranular texture (Abdulzahra and Hadi, 2017) (Fig. 3f).

4.2. Zircon U–Pb geochronology

The zircon grains collected from the MG (Mu11) are transparent and prismatic crystals that are up to 150 μm long. Some grains exhibit microstructures that are visible in cathodoluminescence (CL) images (Fig. 4). They record moderate Th/U ratios (0.66) (Table 1), thus indicating that they record a magmatic origin (Chen et al., 2007; Hartmann and Santos, 2004; Hoskin and Schaltegger, 2003; Rubatto, 2002). The cores and rims of the zoned grains both yield the same ages; they do not have inherited cores. For example, the ages of their cores (e.g., 113.8 ± 4.5 Ma for Mu11-26) and the ages of their rims (e.g., 110.6 ± 4.5 Ma for Mu11-35) are the same, within analytical error (Table 1, Fig. 5). The age of the MG is 111.6 ± 2.4 Ma, with a mean square weighted deviation (MSWD) value of 5.3 (Fig. 5). This crystallization age corresponds to the Middle Cretaceous period (Albian).

4.3. Whole rock geochemistry

The chemical composition data of major element oxides (in weight percent) and trace elements, including REEs (in ppm), are listed in Table 2. These rocks are characterized by their high contents of SiO_2 (70.9–79.6 wt%) and $Na_2O + K_2O$ (5.3–6.5 wt%). These rocks contain 0.4–3.3 wt.% Fe_2O_3, 0.8–2.4 wt.% MgO, 0.1–0.6 wt.% CaO and 0.2–0.4 wt.% TiO_2. The enclave sample (XeMu) records higher concentrations of Al_2O_3, Fe_2O_3 and MgO and lower concentrations of SiO_2 than the MG granites in which it is hosted. All of the MG rocks plot in the granite field, whereas the enclave sample plots in the gabbroic diorite field (Fig. 6a). The MG rocks and the enclave sample exhibit calc-alkaline magma affinity on the AFM diagram (Fig. 6b: Irvine and Baragar, 1971) and are peraluminous, with ASI values of greater than one (Shand, 1943) (Fig. 6c).

The chondrite-normalized REE patterns of the MG rocks and the enclave sample are characterized by enrichment in LREE relative to HREE ($(La/Yb)_N$ = 4.3–11.1), steep negative slopes within LREE ($(La/Sm)_N$ = 2.9–7.2) and flat HREE slopes. Both the MG rocks and the enclave record negative Eu anomalies (Eu/Eu* = 0.5–1.0), which are attributed to feldspar fractionation (Fig. 7a). The geochemical trends defined by the trace elements and REE are consistent, as the primitive mantle-normalized multi-element diagram indicates that the MG rocks and enclave sample are both enriched in Pb, Th, Ba, Zr and LREE (Fig. 7b). The distinct negative Nb, Ta and Ti anomalies observed in the MG rocks are geochemical indicators of subduction-related environments (Pearce et al., 1984). However, the enclave sample is different than its host MG rocks in terms of its contents of Ti, Fe_2O_3, and MgO (Fig. 7b, Table 2). This could be attributed to the differences in their mineralogies, as the enclave sample is more mafic than its MG host rocks. The MG rocks plot in the M-, S- and I- type fields (Fig. 8), with an average 10,000*Ga/Al value that is similar to the reported global average value of I-type granites (Whalen et al., 1987).

Table 2
Major and trace element concentrations of the Mishao granites (MG) and enclave mafic (XeMu).

Sample	Mu5	Mu6	Mu7	Mu8	Mu11	Mu19	Mu23	Mu25	Mu31	XeMu
SiO_2 (%)	75.92	75.33	75.89	79.56	77.76	70.94	71.26	71.05	75.88	50.43
TiO_2	0.27	0.24	0.23	0.16	0.25	0.33	0.34	0.40	0.25	1.26
Al_2O_3	12.84	12.92	13.16	11.20	12.16	14.08	13.38	13.77	12.86	18.19
Fe_2O_3	0.53	1.49	0.99	0.35	0.55	3.19	3.29	3.22	2.20	12.00
MnO	0.02	0.03	0.01	0.02	0.04	0.06	0.10	0.08	0.00	0.22
MgO	1.47	1.55	0.76	0.86	1.54	1.92	2.36	1.90	1.05	7.08
CaO	0.32	0.38	0.55	0.24	0.30	0.33	0.25	0.46	0.09	0.37
Na_2O	6.14	5.43	5.53	5.96	5.86	4.07	3.28	3.20	2.49	4.36
K_2O	0.38	0.71	0.70	0.06	0.22	2.11	2.00	2.55	3.13	0.41
P_2O_5	0.05	0.05	0.05	0.04	0.04	0.07	0.07	0.08	0.02	0.17
H_2O-	0.02	0.05	0.00	0.08	0.19	0.00	0.00	0.18	0.07	1.32
L.O.I	1.13	1.12	1.04	0.56	1.21	1.88	2.57	2.26	1.92	5.29
Total	99.09	99.30	98.90	99.07	100.11	98.97	98.90	99.14	99.96	101.10
V (ppm)	20.6	19.9	15.7	7.6	12.9	26.7	36.2	35.0	28.9	94.1
Cr	1.8	1.3	3.7	1.1	4.8	0.9	0.8	1.0	0.8	1.7
Co	74.1	27.5	31.7	38.5	37.4	14.4	26.6	16.6	17.8	11.6
Ni	2.7	1.7	2.8	2.0	2.3	0.8	0.9	1.2	0.6	1.8
Cu	2.3	1.0	1.2	15.5	1.6	1.4	2.4	3.7	16.7	3.0
Zn	40.3	19.3	10.0	23.2	20.6	47.4	96.2	91.3	25.1	237.2
Ga	19.5	12.1	12.5	8.7	9.1	14.6	14.1	14.2	12.9	19.2
Rb	15.5	15.2	12.8	1.7	3.2	33.9	44.3	45.7	65.7	7.1
Sr	113	74.2	13.7	75.2	62.6	83.4	71.6	74.2	83.6	55.5
Zr	173	93	96	56	78	142	118	124	112	66
Nb	9.3	6.2	5.7	3.8	4.3	5.5	5.1	6.2	4.5	4.0
Cs	0.2	0.2	0.2	0.1	0.1	0.5	0.7	0.7	0.6	0.1
Ba	164	214	233	29	43	461	546	546	4708	119
Pb	2.9	0.8	1.3	0.9	0.9	2.1	5.1	3.6	8.3	4.1
Th	9.3	5.7	5.5	3.8	2.9	3.8	4.1	3.8	3.2	3.1
U	1.8	1.6	0.9	0.7	0.6	1.1	1.6	0.9	1.4	1.4
Y	13.1	10.5	10.7	6.8	6.3	11.3	8.3	13.0	7.6	16.5
La	13.3	20.3	8.23	9.49	6.99	9.87	11.6	16.2	11.5	24.0
Ce	45.6	38.8	18.7	26.3	18.6	23.9	22.3	28.8	23.1	43.1
Pr	4.39	3.61	2.09	2.60	2.15	2.24	2.12	3.10	2.21	4.84
Nd	16.3	12.0	7.70	9.55	7.78	8.40	7.37	11.10	7.81	18.51
Sm	2.73	1.98	1.40	1.80	1.56	1.57	1.05	2.23	1.20	3.33
Eu	0.559	0.603	0.338	0.327	0.332	0.454	0.176	0.708	0.307	0.679
Gd	2.55	1.74	1.51	1.49	1.23	1.73	1.10	2.11	1.06	3.18
Tb	0.401	0.268	0.247	0.202	0.189	0.273	0.181	0.335	0.161	0.449
Dy	2.52	1.73	1.79	1.17	1.23	1.97	1.40	2.32	1.16	3.00
Ho	0.546	0.396	0.381	0.258	0.251	0.429	0.321	0.448	0.250	0.635
Er	1.54	1.12	1.18	0.73	0.74	1.45	1.07	1.49	0.90	1.82
Tm	0.239	0.183	0.196	0.112	0.117	0.242	0.155	0.236	0.145	0.277
Yb	1.96	1.31	1.21	0.77	0.83	1.65	1.18	1.61	1.05	1.77
Lu	0.291	0.237	0.188	0.108	0.120	0.270	0.192	0.273	0.158	0.278
Hf	3.09	2.59	2.87	1.66	2.32	3.82	3.51	3.53	2.98	1.89
Ta	0.64	0.65	0.70	0.51	0.48	0.58	0.54	0.55	0.45	0.20
Eu/Eu*	0.65	1.00	0.71	0.61	0.73	0.85	0.50	1.00	0.84	0.64
$(La/Yb)_N$	4.88	11.12	4.88	8.83	6.04	4.28	7.08	7.22	7.85	9.76
$(La/Sm)_N$	3.44	7.01	10.50	11.40	7.79	4.78	5.62	4.10	30.60	1.86

Eu/Eu*:$Eu_N\sqrt{(Sm_N.Gd_N)}$.

4.4. Sr and Nd isotopic ratios

The initial values of $^{87}Sr/^{86}Sr(i)$ and $^{143}Nd/^{144}Nd(i)$ for the MG rocks are calculated based on their U-Pb zircon age (110 Ma). The $^{143}Nd/^{144}Nd(i)$ ratios range from 0.51235 to 0.51284. Most of the MG samples yield negative εNd(t) values ranging from −2.9 to −1.3, except for sample Mu23, which has a positive εNd(t) value (+6.6) and is thus related to the mantle (Table 3). The measured $^{87}Sr/^{86}Sr(i)$ ratios range from 0.70625 to 0.70740, except for sample Mu7, which has a low $^{87}Sr/^{86}Sr(i)$ ratio of 0.70312 that is consistent with the values of I-type granites (Chappell and White, 1974). The values of the $^{87}Sr/^{86}Sr(i)$ and $^{143}Nd/^{144}Nd(i)$ ratios of the enclave sample are 0.70715 and 0.51240, respectively, and are calculated assuming that its age is identical to that of the host MG granites (Table 3). These values also fall within the range of I-type granites.

5. Discussion

5.1. Magma petrogenesis

In this section we will discuss the magma petrogenesis of the Mishao granites (MG) and their enclave sample (XeMu) in two parts; the source characteristics and the magma evolution.

5.1.1. Source characteristics

According to their geochemical characteristics, the MG rocks and their enclosed enclave sample are I-type granites with the chemical signature of a calc-alkaline magma that formed within a subduction regime (Figs. 6–8). On the Th/Yb–Ta/Yb (Fig. 9a: Pearce and Peate, 1995) and Yb–Th/Ta (Fig. 9b: Gorton and Schandl, 2000) tectonic discrimination diagrams, the MG rocks and the enclave sample show subduction-related active continental margin (ACM) affinity. In addition, these rocks also exhibit magmatic arc affinity; when plotted on the tectonic discrimination diagram of Pearce et al. (1984) (Fig. 9c, d),

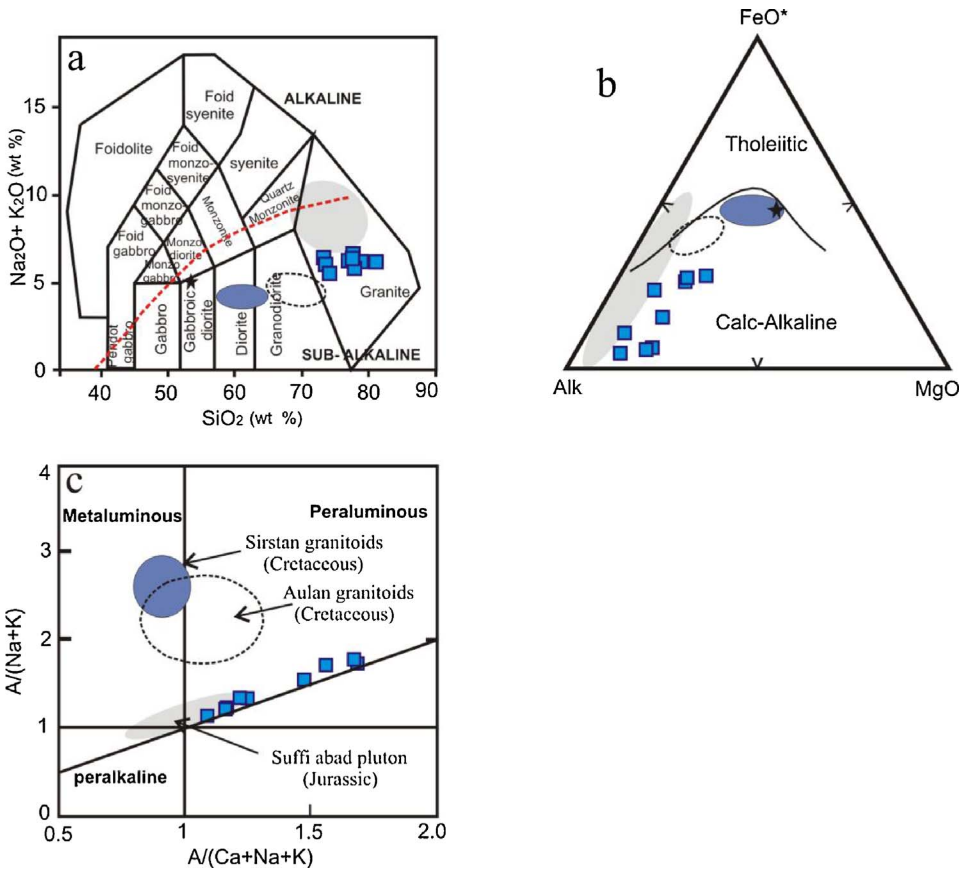

Fig. 6. (a) Alkali-silica diagram (Middlemost, 1985). (b) AFM diagram (Irvine and Baragar, 1971). (c) $Al_2O_3/(CaO + Na_2O + K_2O)$ vs. $Al_2O_3/(Na_2O + K_2O)$ (Shand, 1943). Data from the Suffi abad pluton (Azizi et al., 2011a), Sirstan granitoids (Abdulzahra et al., 2017) and Aulan granitoids (Ali et al., 2016) are shown for comparison. Star symbol represents enclave sample.

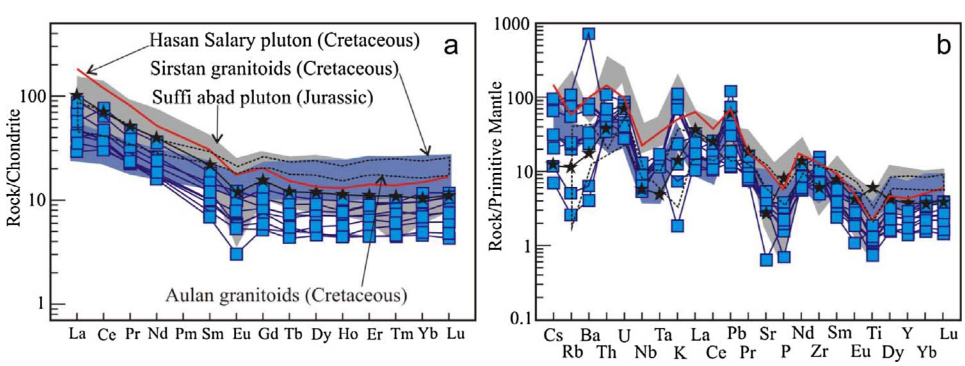

Fig. 7. (a) Chondrite-normalized REE patterns in the MG samples and (b) primitive mantle-normalized trace element spider diagram (normalization after Sun and McDonough, 1989). Data from the Suffi abad pluton (Azizi et al., 2011a), Sirstan granitoids (Abdulzahra et al., 2017), Aulan granitoids (Ali et al., 2016) and Hasan Salary pluton (Mahmoudi et al., 2011) are shown for comparison. Star symbol represents enclave sample.

where they are classified as orogenic granite (Fig. 9e: Abdel-Rahman and El-Kibbi, 2001). Most of the MG rocks and the enclosed enclave sample plot within the mantle array but record a slight shift towards the continental crustal field on the $^{87}Sr/^{86}Sr$ (110 Ma)–εNd (110 Ma) diagram (Fig. 9f), thus indicating that the contribution of crustal components had occurred during the generation of mantle-derived magma. According to these observed geochemical characteristics and relationships, various components, such as the partial melting of subduction-derived materials or a continental crustal component, could have been involved in the generation of the magma that formed the MG rocks. The MG rocks and the enclave sample plot within the mantle array on the $^{87}Sr/^{86}Sr$ (110 Ma)–εNd (110 Ma) diagram and extend towards higher $^{87}Sr/^{86}Sr$ values that plot in the continental crust area (Fig. 9f); however, their $^{143}Nd/^{144}Nd$ ratios remain almost constant (Table 3). These relationships suggest that the subduction-derived magma has been variably contaminated with a crustal component. In addition, the observed enrichments of LREE, Th and LILE in the MG rocks reflect the involvement of a multi-component source magma.

Although the initial values of the $^{87}Sr/^{86}Sr$ ratios of the MG rocks range from 0.7074 to 0.7062, thus indicating that these rocks have an I-type granite origin. Some authors have suggested a critical boundary of an $^{87}Sr/^{86}Sr$ value of 0.7060 for I-type granites with initial $^{87}Sr/^{86}Sr$ ratios ranging from 0.7040 to 0.7060 (Armstrong et al., 1977; Chappell and White, 1974). The slightly higher values of the initial $^{87}Sr/^{86}Sr$ ratios of the MG rocks most likely reflect the influence of the whole-rock Rb-Sr isotopic disturbance that occurred during the secondary events of deformation, alteration and/or metamorphism (e.g., Allegre, 2008; Asmeron et al., 1991; Greenough and Fryer, 1991). Evidence of variable degrees of the resetting of the Rb-Sr isotopic system in the SaSZ has previously been reported; this resetting has been linked to the reactivation of these rocks during secondary processes (e.g., Abdulzahra et al., 2016, 2017; Bea et al., 2011; Masoudi et al., 2002). For example, Abdulzahra et al. (2017) documented the resetting of the Rb-Sr isotopic system within the Sirstan granitoid rocks in the Shalair Valley area. They obtained two different ages of the Sirstan granitoids, 110 Ma and 52.4 Ma, using U-Pb zircon age analysis and Rb-Sr isochron dating, respectively. They interpreted the age of the whole-rock Rb-Sr isochron to represent evidence of isotopic resetting linked to the reactivation of

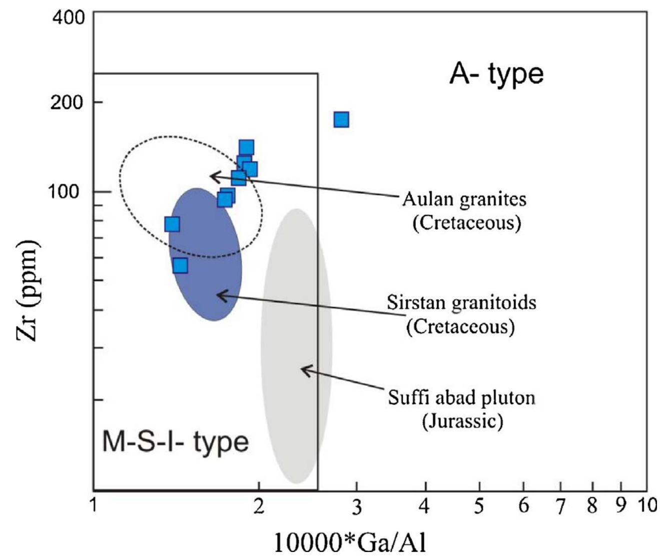

Fig. 8. 10000*Ga/Al versus Zr (Whalen et al., 1987) for the MG rocks. Data from the Suffi abad pluton (Azizi et al., 2011a), Sirstan granitoids (Abdulzahra et al., 2017) and Aulan granitoids (Ali et al., 2016) are shown for comparison.

the Sirstan granitoids due to the collision between the Arabian and Iranian plates that occurred during the Early Eocene.

As previously noted, the geochemical characteristics and clumped distribution within the mantle array on the $^{87}Sr/^{86}Sr$ (110 Ma)–εNd (110 Ma) diagram (Fig. 9f) indicate that the magma source of the MG rocks and the enclave sample record the influence of continental materials and/or subduction-released fluids in the continental margin zone. Furthermore, these rocks record distinct Nb, Ta and Ti depletions, thus recording the geochemical characteristics of subduction-related calc-alkaline magma (Pearce et al., 1984).

The similarities in the major and trace elements and Sr-Nd isotopic compositions of the enclave and the enclosing MG granites most likely suggest that these rocks have a cogenetic origin. On the other hand, the mineralogical and geochemical characteristics of the enclave indicate that the enclave is more mafic (SiO_2 = 50.4 wt%) than the hosted rocks, as it contains a greater abundance of amphibole and chlorite than the hosted granites. These lines of evidence could suggest that the enclave is the remaining representative of the early stage of a fractionated precursor and thus represents a less evolved portion of the original magma. The theory that this enclave is associated with the granitoid rocks has deemed controversial by many authors, because it plays an important role in the evolution of granitic magmas (Barbarin, 1988; Barbarin and Didier, 1992; Chappell et al., 1987; Chen et al., 1990; Elburg, 1996; Kocak, 2006). More detailed analyses concerning the radiometric age and petrogenesis of the enclaves in the MG rocks are required to better understand the relationship between the enclaves and the hosted granites.

5.1.2. Magma evolution

The Mishao granites show a narrow range of silica contents, indicating that these rocks came from the same magma source (Fig. 10a–l). The samples show relatively linear trends of SiO_2 with the major and trace elements, all support the fractional crystallization during the magma evolution of the MG rocks. The negative correlation between SiO_2 and Al_2O_3 contents with the prominently negative Eu anomalies (Fig. 10c, Fig. 7b), indicate the role of plagioclase in fractional crystallization processes during the magma evolution of the MG rocks. The scattered plots (e.g. Na_2O and CaO; Fig. 10) are probably attributed to the mobility of these elements during alteration processes. The initial $^{87}Sr/^{86}Sr$ (110Ma) and εNd (110Ma) values of the MG samples exhibit neither negative nor positive correlation trends with increasing SiO_2 contents, suggesting the fractional crystallization and/or partial melting control in their generation (Figs. 11a–b). However, the MG rocks have high SiO_2 contents (< 70 wt%); therefore, they cannot be directly derived from partial melting of a mantle source. Moreover, in the La (ppm) versus $(La/Yb)_N$ diagram (Fig. 11c), the MG rocks show a horizontal trend, implying that the fractional crystallization had played a major role in the magma evolution of the MG rocks.

Samples from the MG and the enclave sample (XeMu) exhibit strong evidence for crustal contamination (Figs. 11d, e). Additional role on crustal contamination is apparent in Fig. 11f, where the Mishao granites and the enclave sample (XeMu) are plotted between the primitive mantle and close to the continental crust composition. Figs. 11e, f also illustrate that the MG rocks have undergone greater degree of crustal contamination by upper crust than the Sirstan and Aulan I-type granites of the Shalair Valley area. It is likely for the MG rocks that both fractional crystallization and crustal contamination are involved in the generation of the magma. Therefore, we infer that a combination of fractional crystallization and contamination by upper crust contributed to the generation of the magma for the MG rocks.

5.2. Geodynamic implications and tectonic setting

The Middle Jurassic-Early Cretaceous Period represents the most intensive period of magmatic activity that had occured along the active continental margin in the SaSZ. These magmatic activities are linked to the subduction of the Neo-Tethys Ocean beneath the Iranian Plate (e.g., Agard et al., 2005; Berberian and Berberian, 1981; Berberian and King, 1981; Hassanzadeh and Wernicke, 2016; Sengor, 1990; Sepahi et al., 2014; Shakerardakani et al., 2015; Fazlnia et al., 2009). Evidence of Cretaceous calc-alkaline magmatic activity is well developed in the northwestern region of the SaSZ, with its geochemical characteristics exhibiting an active continental margin affinity (Azizi and Jahangiri,

Table 3
Sr-Nd isotope ratios for whole-rock samples from the Mishao granites (MG) and enclave mafic (XeMu).

Sample	$^{87}Rb/^{86}Sr$	$^{87}Sr/^{86}Sr$	± 2 S.E.	$^{147}Sm/^{144}Nd$	$^{143}Nd/^{144}Nd$	± 2 S.E.	$^{87}Sr/^{86}Sr(i)$	$^{143}Nd/^{144}Nd(i)$	Σ_{Nd} (t = 110)
Mu5	0.396	0.707939	0.000011	0.101	0.512456	0.000007	0.70732	0.51238	−2.2
Mu6	0.591	0.708249	0.000011	0.100	0.512419	0.000008	0.70732	0.51235	−2.9
Mu7	2.70	0.707345	0.000011	0.110	0.512464	0.000008	0.70312	0.51238	−2.2
Mu8	0.0638	0.707501	0.000014	0.114	0.512455	0.000008	0.70740	0.51237	−2.4
Mu11	0.146	0.707576	0.000012	0.121	0.512474	0.000008	0.70735	0.51239	−2.1
Mu19	1.18	0.708638	0.000014	0.113	0.512510	0.000008	0.70680	0.51243	−1.3
Mu23	1.79	0.709176	0.000014	0.0860	0.512898	0.000009	0.70637	0.51284	6.6
Mu25	1.78	0.709037	0.000012	0.121	0.512486	0.000008	0.70625	0.51240	−1.9
Mu31	2.27	0.710674	0.000011	0.0927	0.512482	0.000008	0.70712	0.51242	−1.6
XeMu	0.369	0.707722	0.000011	0.109	0.512474	0.000008	0.70715	0.51240	−2.0

The Sr and Nd natural isotope ratios were normalized based on $^{86}Sr/^{88}Sr$ = 0.1194 and $^{146}Nd/^{144}Nd$ = 0.7219. The average and 1σ for the isotope ratio standards are JNdi–1 = 0.512097 ± 0.000010 (n = 13) and for NBS987 = 0.710240 ± 0.000010 (n = 17). CHUR (Chondritic Uniform Reservoir) values, $^{147}Sm/^{144}Nd$ = 0.1967 and $^{143}Nd/^{144}Nd$ = 0.512638, were used to calculate εNd (DePaolo and Wasserburg, 1976).

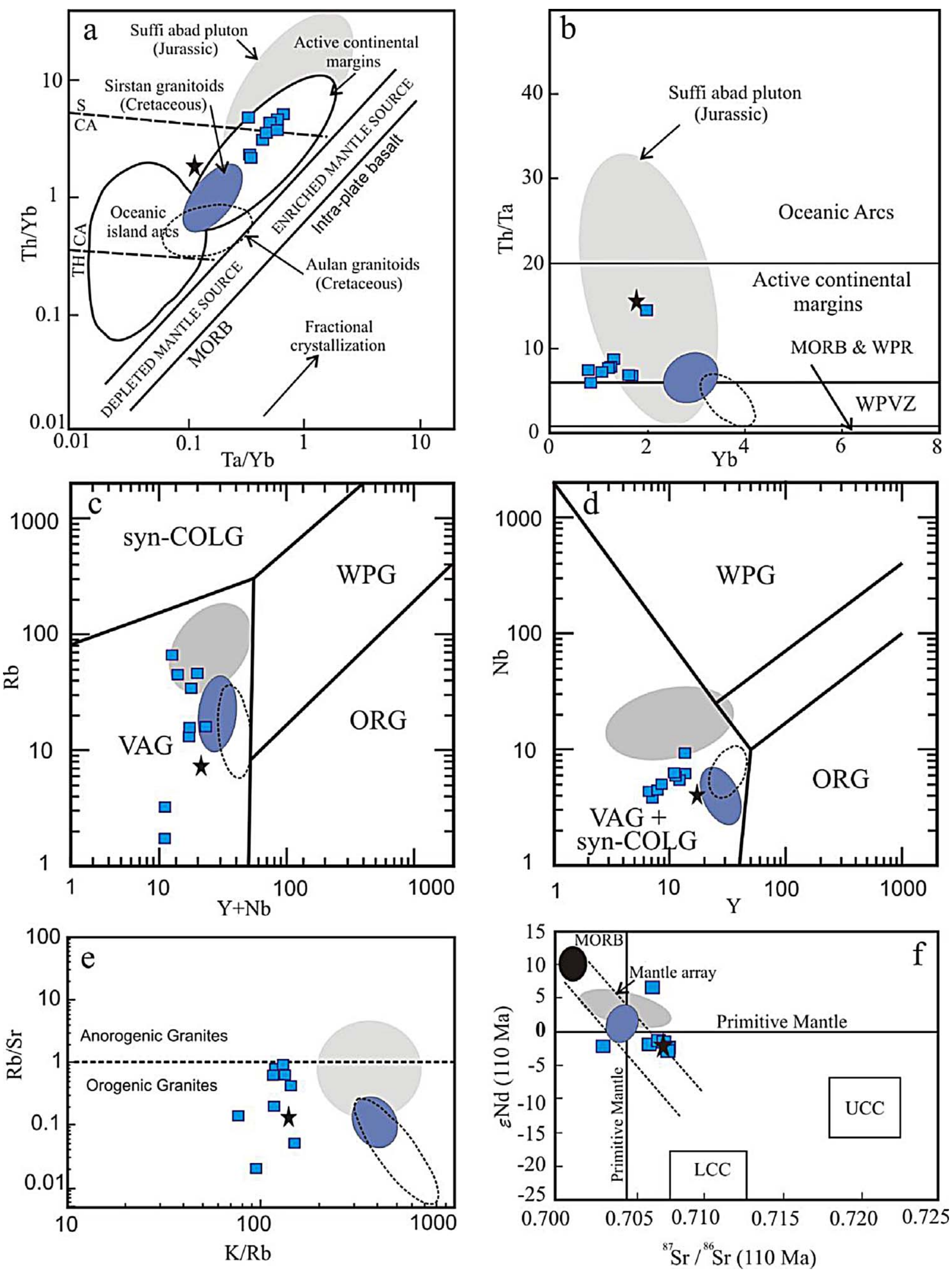

Fig. 9. (a) Ta/Yb vs. Th/Yb (Pearce and Peate, 1995), (b) Yb vs. Th/Ta (Gorton and Schandl, 2000), (c) Y + Nb vs. Rb, (d) Y vs. Nb (Pearce et al., 1984), (e) Rb/Sr vs. K/Rb (Abdel-Rahman and El-Kibbi, 2001) and (f) $^{87}Sr/^{86}Sr$ (110 Ma) vs. εNd (110 Ma) for the MG rock samples. Data from the Suffi abad pluton (Azizi et al., 2011a), Sirstan granitoids (Abdulzahra et al., 2017) and Aulan granitoids (Ali et al., 2016) are shown for comparison. Star symbol represents enclave sample. UCC: upper continental crust; LCC: lower continental crust; ORG: ocean ridge granite; syn-COLG: syn-collisional granite; VAG: volcanic arc granite; WPG: within-plate granite.

2008; Azizi and Moinevaziri, 2009; Mohajjel et al., 2003; Moinevaziri et al., 2015). Towards the southeastern region of the SaSZ, Cretaceous magmatism is much less exposed and comprises intermediate volcanic rocks (Mohajjel et al., 2003).

During the Middle Cretaceous Period, the northeastwards movement of the Afro-Arabian Plate became more rapid as the result of accelerated Atlantic spreading (Sharland et al., 2001). This became faster in the Middle Turonian with the development of a supra-subduction zone ophiolite in northeastern Iraq and northwestern Iran; during the Late Cretaceous Period (e.g., Agard et al., 2005, 2011; Ali et al., 2012; Shafaii Mogadam et al., 2009, 2014). Although Middle to Late Cretaceous granitoid rocks are poorly documented in theSaSZ (Chiu et al., 2013), other studies have recently reported about the presence of Middle to Late Cretaceous granitoid rocks. In the SaSZ of Iraq (i.e., the Shalair Valley area), Middle Cretaceous U-Pb zircon ages have been reported; the Sirstan granites in the Shalair Valley area yield zircon U-Pb ages ranging from 109.3 ± 1.3 Ma to 114.9 ± 4.9 Ma (Fig. 1b) (Abdulzahra et al., 2017). These rocks are I-type granites with microgranular mafic enclaves and are metaluminous with calc-alkaline affinity. Their geochemical characteristics, including their Sr-Nd isotopic compositions, indicate that the Sirstan granites were generated in an active continental margin regime; located over a subduction zone (Abdulzahra et al., 2017). The geochemical data of the Sirstan granitoids indicate that these rocks are less evolved and contaminated than the MG rocks (Figs. 9–11). Therefore, the Sirstan granitoids were most likely intruded into deeper crustal levels within the rocks of the Katar-Rash Volcanic Series than the MG body was. In the SaSZ of Iran, the Hasan Salary I-type granites yield a zircon U-Pb age of 108.8 ± 0.3 Ma (Mahmoudi et al., 2011); Mazhari et al. (2011) dated the Naqadeh complex and reported a crystallization age of 96 ± 2.3 Ma (Fig. 1a). The results of all these studies, performed along the SaSZ and covering northeastern part of Iraq and northwestern Iran, suggest that these granitoid rocks are related to the subduction-related magmatism of the Neo-Tethys Ocean in an active continental margin regime along the northwestern part of the SaSZ. The Mishao granites were intruded into the rocks of the Katar-Rash Volcanic Series (Fig. 1b), which is composed

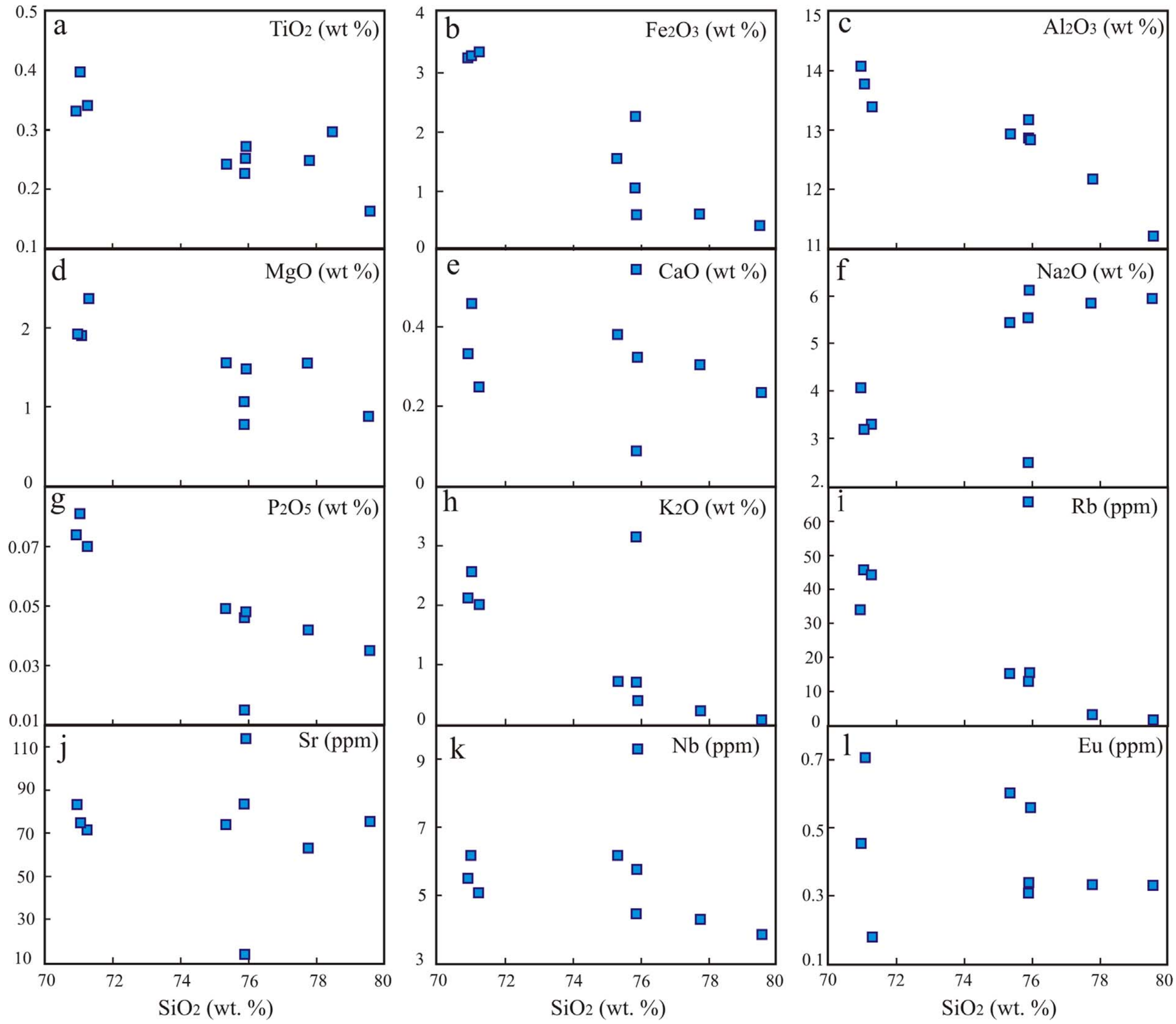

Fig. 10. Harker variation diagrams for the MG rock samples.

of basalts and andesites with lesser amounts of rhyolite (Ali et al., 2016). The presence of rhyolite with high concentrations of SiO_2, K_2O and Zr in this unit suggests that these rocks were influenced by continental materials and were linked to the active continental margin during the subduction of the Neo-Tethys Ocean beneath the Iranian Plate (Buday and Jassim, 1987; Jassim and Goff, 2006). It is likely that the Mishao granites were more evolved or intruded at shallow levels in the crust within the rocks of the Katar-Rash Volcanic Series and thus suffered more differentiation or a greater degree of contamination from the continental crust than the Sirstan and Aulan bodies (Fig. 1b). Most of the granitoid rocks located in the SaSZ have been interpreted to have formed in the active margin and are linked to the subduction of the Neo-Tethys Ocean beneath the SaSZ with a predominantly calc-alkaline affinity during the Jurassic-Tertiary Period (e.g., Berberian and King, 1981; Ghasemi and Talbot, 2006; Sengor, 1990; Fazlnia et al., 2009).

As noted above, the geochemical and Sr-Nd isotopic data of the MG rocks indicate that these rocks are formed from subduction-related calcalkaline magma above a subduction zone. This magma was then subjected to contamination by crustal materials during its upwelling and ascent into high levels within the continental crust. These features strongly suggest that the MG rocks originated from a magmatic arc linked to an active continental margin (Fig. 12; modified after Ali et al., 2013; Ghasemi and Talbot, 2006).

6. Conclusions

The Mishao granitic rocks are porphyritic I-type peraluminous granites with microgranular mafic enclaves. The results of zircon U-Pb dating indicate that these rocks were crystallized at 111.6 ± 2.4 Ma. The geochemical characteristics and Sr-Nd isotopic compositions of these rocks indicate that the MG rocks are subduction-related calc-alkaline granites, which were generated in an active continental margin regime. The present study demonstrates the existence of Middle Cretaceous igneous activity and thus reduces the magmatic gap observed in the SaSZ during this time.

Acknowledgements

The first author would like to thank Nagoya University in Japan for supporting him as a Special Research Student during the period of Nov. 2014 to Oct. 2015 and the Iraq Geological Survey for their support during field trips. We also thank Ms. Masumi Nozaki (Nagoya University Museum) for SEM analysis, Prof. Makoto Takeuchi (Nagoya University) for zircon separation and Mr. Yoshikazu Kouchi (Toyama University, Japan) for advice about U–Pb age calculations. This work was financially supported by the JSPS KAKENHI grants (no. 25303029 and no. 17H01671) in Japan and the Ministry of Higher Education and Scientific Research in Iraq. We are grateful to the editor-in-chief, Alex Deutsch, H. Shafaii Moghadam, Associate Editor and anonymous

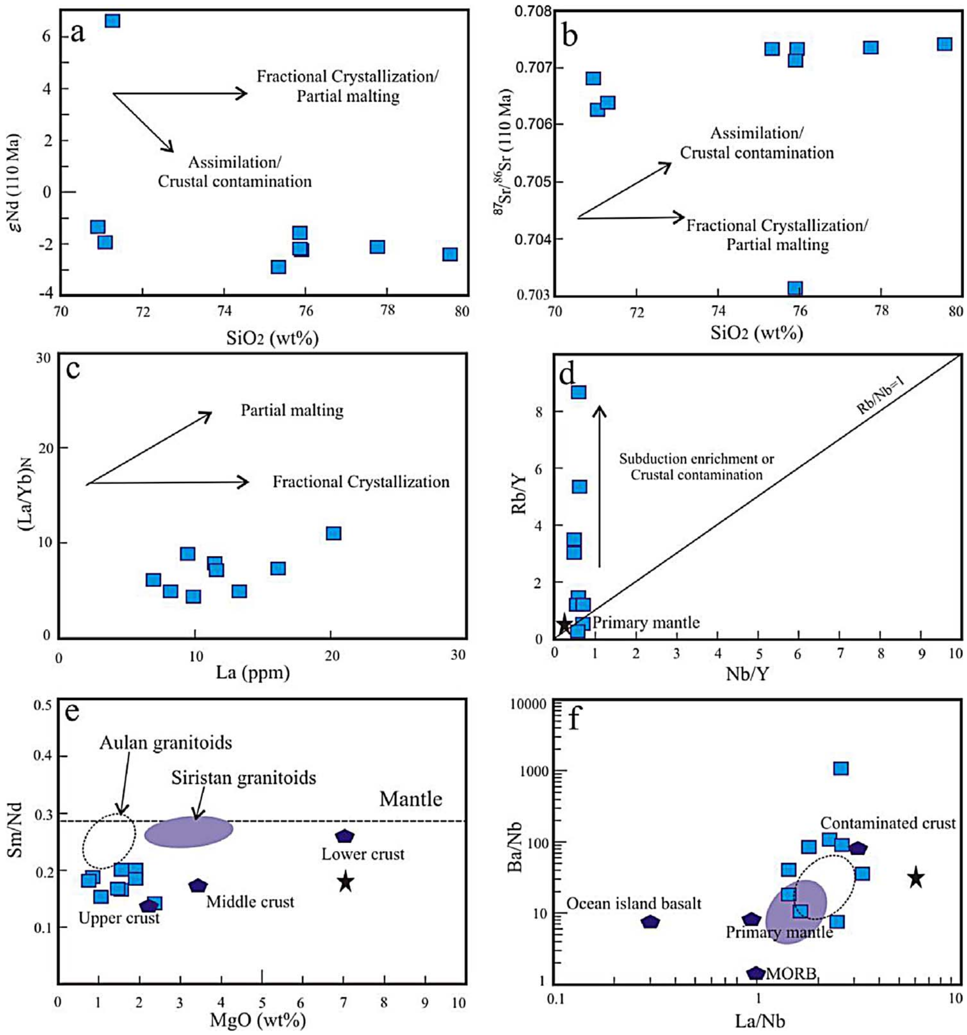

Fig. 11. Plots of (a) εNd versus SiO_2; (b) $^{87}Sr/^{86}Sr$ (100 Ma) versus SiO_2; (c) (La/Yb)N versus La (ppm) (d) Rb/Y versu Nb/Y; (e) Sm/Nd versus MgO (Nicholson et al., 2010); (f) Ba/Nb versus La/Nb (from Maghdour-Mashhour et al., 2015) diagrams for the MG rocks. Data from the Sirstan granitoids (Abdulzahra et al., 2017) and Aulan granitoids (Ali et al., 2016) are shown for comparison.

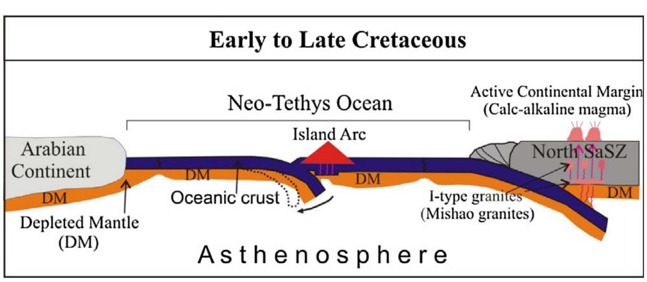

Fig. 12. Simplified schematic cross-section for evolution of the Mishao granites.

reviewers for their constructive comments to improve our paper.

References

Abdel-Rahman, A.M., El-Kibbi, M.M., 2001. Anorogenic magmatism: chemical evolution of the Mount El-Sibai A-type complex (Egypt), and implications for the origin of within-plate felsic magmas. Geol. Mag. 138, 67–85.

Abdulzahra, I.K., Hadi, A., 2017. Petrology of the granitoid intrusions in the Shalair Valley area, northeastern Iraq. Iraqi J. Sci. 58, 88–102.

Abdulzahra, I.K., Hadi, A., Asahara, Y., Azizi, H., Yamamoto, K., 2016. Zircon U-Pb ages and geochemistry of Devonian A-type granites in the Iraqi Zagros suture zone (Damamna area): New evidence for magmatic activity related to the Hercynian Orogeny. Lithos 264, 360–374.

Abdulzahra, I.K., Hadi, A., Azizi, H., Asahara, Y., Yamamoto, K., 2017. Zircon U-Pb ages and Sr-Nd isotope ratios for Sirstan granitoid body, NE Iraq: evidence for magmatic activity in the Middle Cretaceous Period. C.R. Geosci. 349, 53–62.

Agard, P., Omrani, J., Jolivet, L., Mouthereau, F., 2005. Convergence history across Zagros (Iran): constraints from collisional and earlier deformation. Geologische Rundschau 94, 401–419.

Agard, P., Omrani, J., Jolivet, L., Whitechurch, H., Vrielynck, B., Spakman, W., Monie, P., Meyer, B., Wortel, R., 2011. Zagros orogeny: a subduction-dominated process. Geol. Mag. 148, 692–725.

Ahmadi Khalaji, A., Esmaeily, D., Valizadeh, M.V., Rahimpour-Bonab, H., 2007. Petrology and geochemistry of the granitoid complex of Boroujerd, Sanandaj–Sirjan Zone, Western Iran. J. Asian Earth Sci. 29, 859–877.

Al-Shible, T.A., Kettaneh, Y.A., 1972. Reconnaissance Radiometric and Geology in NE Penjwin (Shalair Valley). Iraqi Atomic Energy Commission Report. pp. 36.

Alavi, M., 1980. Tectonostratigraphic evolution of zagrosides of Iran. Geology 8, 144–149.

Alavi, M., 1994. Tectonic of the Zagros orogenic belt of Iran: new data and interpretations. Tectonophysics 229, 211–238.

Alavi, M., 2004. Regional stratigraphy of the Zagros fold-thrust belt of Iran and its pro-foreland evolution. Am. J. Sci. 304 (1), 1–20.

Ali, S.A., Buckman, S., Aswad, K.J., Jones, B.G., Ismail, S.A., Nutman, A.P., 2012. Recognition of Late Cretaceous Hasanbag ophiolite-arc rocks in the Kurdistan Region of the Iraqi Zagros suture zone: a missing link in the paleogeography of the closing Neotethys Ocean. Lithosphere 4, 395–410.

Ali, S.A., Buckman, S., Aswad, K.J., Jones, B.G., Ismail, S., Nutman, A.P., 2013. The tectonic evolution of a neo-tethyan (Eocene–Oligocene) islandarc (Walash–Naopurdan group) in the Kurdistan region of the NE Iraqi Zagros Thrust Zone. Isl. Arc J. 22, 104–125.

Ali, S.A., Ismail, S.A., Nutman, A.P., Bennett, V.C., Jones, B.G., Buckman, S., 2016. The intra-oceanic Cretaceous (~108 Ma) Kata–Rash arc fragment in the Kurdistan segment of Iraqi Zagros suture zone: implications for Neotethys evolution and closure. Lithos 260, 154–163.

Alirezaei, S., Hassanzadeh, J., 2012. Geochemistry and zircon geochronology of the Permian A-type Hasanrobat granite, Sanandaj–Sirjan belt: a new record of the Gondwana break-up in Iran. Lithos 151, 122–134.

Allahyari, K., Saccani, E., Pourmoafi, M., Beccaluva, L., Masoudi, F., 2010. Petrology of mantle peridotites and intrusive mafic rocks from the Kermanshah ophiolitic complex (Zagros belt, Iran): implications for the geodynamic evolution of the Neo-Tethyan oceanic branch between Arabia and Iran. Ofioliti 35, 71–90.

Allegre, C.J., 2008. Isotope Geology. Cambridge University Press, Cambridge, pp. 512.

Armstrong, R.L., Taubeneck, W.H., Hales, P.O., 1977. Rb–Sr and K–Ar geochronometry of Mesozoic granitic rocks and their Sr isotopic composition, Oregon, Washington, and Idaho. Geol. Soc. Am. Bull. 88, 397–411.

Asmeron, Y., Damon, P., Dickinson, W.R., Zartman, R.E., 1991. Resetting of Rb-Sr ages of volcanic rocks by low grade burial metamorphism. Chem. Geol. (Isot. Geosci. Sect.) 87, 167–173.

Azizi, H., Asahara, Y., 2013. Juvenile granite in the Sanandaj-Sirjan zone, NW Iran:Late Jurassic–Early cretaceous arc-continent collision. Int. Geol. Rev. 55, 1523–1540.

Azizi, H., Jahangiri, A., 2008. Cretaceous subduction-related volcanism in the northern Sanandaj-Sirjan Zone, Iran. J. Geodyn. 45, 178–190.

Azizi, H., Moinevaziri, H., 2009. Review of the tectonic setting of Cretaceous to Quaternary volcanism in northwestern Iran. J. Geodyn. 47, 167–179.

Azizi, H., Asahara, Y., Mehrabi, B., Chung, S.L., 2011a. Geochronological and geochemical constraints on the petrogenesis of high-K granite from the Suffi abad area, Sanandaj–Sirjan zone, NW Iran. Chemie der Erde 71, 363–376.

Azizi, H., Tanaka, T., Asahara, Y., Chung, S.-L., Zarrinkoub, M.H., 2011b. Discrimination of the age and tectonic setting for magmatic rocks along the Zagros thrust zone, northwest Iran, using the zircon U–Pb age and Sr-Nd isotopes. J. Geodyn. 52, 304–320.

Azizi, H., Beiranvand, M.Z., Asahara, Y., 2015. Zircon U–Pb ages and petrogenesis of a tonalite–trondhjemite–granodiorite (TTG) complex in the northern Sanandaj–Sirjan zone, northwest Iran: evidence for Late Jurassic arc–continent collision. Lithos 216–217, 178–195.

Barbarin, B., Didier, J., 1992. Genesis and evolution of mafic microgranular enclaves through various types of interaction between coexisting felsic and mafic magmas. Trans. Royal Soc. Edinburgh Earth Sci. 83, 145–153.

Barbarin, B., 1988. Field evidence for successive mixing and mingling between the Piolard Diorite and the Saint-Julien-la-Vetre Monzogranite (Nord-Forez, Massif Central, France). Can. J. Earth Sci. 25, 49–59.

Bea, F., Mazhari, A., Montero, P., Amini, S., Ghalamghash, J., 2011. Zircon dating, Sr and Nd isotopes, and element geochemistry of the Khalifan pluton, NW Iran: evidence for Variscan magmatism in a supposedly Cimmerian superterrane. J. Asian Earth Sci. 40, 172–179.

Berberian, F., Berberian, N.M., 1981. Tectono-Plutonic Episodes in Iran. In Zagros-Hindu Kush-Himalaya Geodynamic Evolution, vol. 3. American Geophysical Union, Washington, D.C, pp. 5–32.

Berberian, M., King, C.C.P., 1981. Toward a paleogeography and tectonic evolution of Iran. Can. J. Earth Sci. 18, 210–265.

Buday, T., Jassim, S.Z., 1987. The Regional Geology of Iraq, Vol. 2, Tectonism, Magmatism and Metamorphism. Geologial Survey and Mineral Investigation. Baghdad, Iraq. pp. 352.

Buday, T., 1980. The Regional Geology of Iraq, Vol. 1, Stratigraphy and Palegeography. Geologial Survey and Mineral Investigation. Baghdad, Iraq. pp. 445.

Chappell, B.W., White, A.J.R., 1974. Two contrasting granite types. Pac. Geol. 8, 173–174.

Chappell, B.W., White, A.J.R., Wyborn, D., 1987. The importance of residual source material (restite) in granite petrogenesis. J. Petrol. 28, 1111–1138.

Chen, Y.D., Price, R.C., White, A.J.R., Chappell, B.W., 1990. Mafic inclusions from the glenbog and blue gum granite suites, southeastern Australia. J. Geophys. Res. 95, 17757–17785.

Chen, R.X., Zheng, Y.F., Zhao, Z.F., Tang, J., Wu, F.Y., Liu, X.M., 2007. Zircon U–Pb ages and Hf isotopes in ultrahigh-pressure metamorphic rocks from the Chinese Continental Scientific Drilling project. J. Metamorph. Geol. 25, 873–894.

Chiu, H.-Y., Chung, S., Zarrinkoub, M.H., Mohammadi, S.S., Khatib, M.M., Iizuka, Y., 2013. Zircon U–Pb age constraints from Iran on the magmatic evolution related to Neotethyan subduction and Zagros orogeny. Lithos 162–163, 70–87.

De Villiers, P.R., 1957. The Geology of the Shaliar Valley Unpublished Report, Geologial Survey and Mineral Investigation. Baghdad, Report No 270/52.

DePaolo, D.J., Wasserburg, G.J., 1976. Nd isotopic variations and petrogenetic models. Geophys. Res. Lett. 3, 249–252.

Dewey, J.F., Pitman, W.C., Pyan, W.B.F., Bonin, J., 1973. Plate tectonic and the evolution of the Alpine system. Geol. Soc. Am. Bull. 84, 3137–3180.

Elburg, M.A., 1996. Evidence of isotopic equilibration between microgranitoid enclaves and host granodiorite Warburton Granodiorite, Lachlan Fold Belt, Australia. Lithos 38, 1–22.

Esna-Ashari, A., Tiepolo, M., Valizadeh, M.-V., Hassanzadeh, J., Sepahi, A.-A., 2012. Geochemistry and zircon U–Pb geochronology of aligoodarz granitoid complex, Sanandaj-Sirjan zone, Iran. J. Asian Earth Sci. 43, 11–22.

Fazlnia, A., Schenk, V., van der Straaten, F., Mirmohammadi, M., 2009. Petrology, geochemistry, and geochronology of trondhjemites from the Qori Complex, Neyriz, Iran. Lithos 112, 413–433.

Fouad, S.F.A., 2014. Western Zagros fold-thrust belt, part II: the high folded zone. Iraqi Bull. Geol. Min. 53–71.

Fouad, S.F.A., 2015. Tectonic map of Iraq scale 1:1000000, 3rd ed., 2012. Iraqi Bull. Geol. Min. 11 (1), 1–7.

Ghasemi, A., Talbot, C.J., 2006. A new tectonic scenario for the Sanandaj-Sirjan Zone (Iran). J. Asian Earth Sci. 26, 683–693.

Goolaerts, A., Mattielli, N., De Jong, J., Weis, D., Scoates, J.S., 2004. Hf and Lu reference values for the zircon standard 91500 by MCICP-MS. Chem. Geol. 206, 1–9.

Gorton, M.P., Schandl, E.S., 2000. From continents to island arcs: a geochemical index of tectonic setting for arc-related and within-plate felsic to intermediate volcanic rocks. Can. Mineral. 38, 1065–1073.

Greenough, J.D., Fryer, B.J., 1991. Nd and Sr isotopic composition of the lamprophyric Malpeque Bay Sill, Prince Edward Island. Can. Mineral. 29, 311–317.

Hartmann, L.A., Santos, J.O.S., 2004. Predominance of high Th/U, magmatic zircon in Brazilian Shield sandstones. Geology 32, 73–76.

Hassanzadeh, J., Wernicke, B.P., 2016. The Neotethyan Sanandaj-Sirjan zone of Iran as an archetype for passive margin-arc transitions. Tectonics 35, 586–621.

Hassanzadeh, J., Stockli, D.F., Horton, B.K., Axen, G.J., Stockli, L.D., Grove, M., Schmitt, A.K., Walker, J.D., 2008. U–Pb zircon geochronology of late Neoproterozoic–Early Cambrian granitoids in Iran: implications for paleogeography, magmatism, and exhumation history of Iranian basement. Tectonophysics 451, 71–96.

Haynes, S.J., McQuillan, H., 1974. Evolution of the zagros suture zone, southern Iran. Geol. Soc. Am. Bull. 85, 739–744.

Hoskin, P.W.O., Schaltegger, U., 2003. The composition of zircon and igneous and metamorphic petrogenesis. Rev. Mineral. Geochem. 53, 27–62.

Irvine, T.N., Baragar, W.R.A., 1971. A guide to the chemical classification of the common volcanic rocks. Can. J. Earth Sci. 8, 523–548.

Jassim, S.Z., Goff, J.C., 2006. Geology of Iraq. Dolin, Parague and Moravian Museum Brno, pp. 341p–$9.

Kocak, K., 2006. Hybridization of mafic microgranular enclaves: mineral and whole-rock chemistry evidence from the Karamadazi Granitoid, Central Turkey. Int. J. Earth Sci. 95, 587–607.

Kouchi, Y., Orihashi, Y., Obara, H., Fujimoto, T., Haruta, Y., Yamamoto, K., 2015. Zircon U-Pb dating by 213 nm Nd: YAG laser ablation inductively coupled plasma mass spectrometry: optimization of the analytical condition to used NIST SRM 610 for Pb/U fractionation correction. Chikyukagaku (Geochem.) 49, 19–35 (in Japanese with English abstract).

Ludwig, K.R., 2012. Isoplot, A Geochronological Toolkit for Microsoft Excel 5. Berkeley Geochronology Center, Special Publication, pp. 75.

Maghdour-Mashhour, R., Esmaeily, D., Shabani, A.A.T., Chiaradia, M., Latypov, R., 2015. Petrology and geochemistry of the Karaj Dam basement sill: implications for geodynamic evolution of the Alborz magmatic belt. Chemie der Erde 75, 237–260.

Mahmoudi, S., Corfu, F., Masoudi, F., Mehrabi, B., Mohajjel, M., 2011. U–Pb dating and emplacement history of granitoid plutons in the Northern Sanandaj–Sirjan zone, Iran. J. Asian Earth Sci. 41, 238–249.

Masoudi, F., Yardley, B.W.D., Cliff, R.A., 2002. Rb–Sr geochronology of pegmatites, plutonic rocks and a hornfels in the region southwest of Arak, Iran. J. Sci. Islamic Republic Iran 13, 249–254.

Mazhari, S.A., Bea, F., Amini, S., Ghalamghash, J., Molina, J.F., Montero, P., Scarrow, J.H., Williams, I.S., 2009. The Eocene bimodal Piranshahr massif of the Sanadaj-Sirjan Zone West Iran: a marker of the end of collision in the Zagros orogen. J. Geol. Soc. London 166, 53–69.

Mazhari, S.A., Amini, S., Ghalamghash, J., Bea, F., 2011. Petrogenesis of granitic unit of naqadeh complex, Sanandaj-Sirjan zone, NW Iran. Arabian J. Geosci. 4, 59–67.

Middlemost, E.A.K., 1985. Magmas and Magmatic Rocks. Longman, London, pp. 266.

Mohajjel, M., Fergusson, C.L., Sahandi, M.R., 2003. Cretaceous–tertiary convergence and continental collision, Sanandaj-Sirjan zone, western Iran. J. Asian Earth Sci. 21, 397–412.

Moinevaziri, H., Akbarpour, A., Azizi, H., 2015. Mesozoic magmatism in the northwestern Sanandaj–Sirjan zone as an evidence for active continental margin. Arabian J. Geosci. 8, 3077–3088.

Nicholson, K.N., Khan, M., Mahmood, K., 2010. Geochemistry of the Chagai-Raskoh arc Pakistan: complex arc dynamics spanning the Cretaceous to the Quaternary. Lithos 118, 338–348.

Orihashi, Y., Nakai, S., Hirata, T., 2008. U-Pb Age determination for seven standard zircons using inductively coupled plasma–mass spectrometry coupled with frequency quintupled Nd-YAG ($\lambda = 213$ nm) laser ablation system: comparison with LA-ICP-MS zircon analyses with a NIST glass reference material. Resour. Geol. 58, 101–123.

Pearce, J.A., Peate, D.W., 1995. Tectonic implications of the composition of volcanic arc magmas. Ann. Rev. Earth Planet. Sci. 23, 251–285.

Pearce, J.A., Harris, N.B.W., Tindle, A.G., 1984. Trace-element discrimination diagrams for the tectonic interpretation of granitic-rocks. J. Petrol. 25, 956–983.

Rubatto, D., 2002. Zircon trace element geochemistry: partitioning with garnet and the link between U–Pb ages and metamorphism. Chem. Geol. 184, 123–138.

Sengor, A.M.C., 1990. A New Model for the Late Paleozoic-Mesozoic Tectonic Evolution of Iran and Implications for Oman 49. Geological Society London, pp. 797–831 Special. Publication.

Sepahi, A.-A., Shahbzi, H., Siebel, W., Ranin, A., 2014. Geochronology of plutonic rocks from the Sanandaj-Sirjan zone, Iran and new zircon and titanite U-Th-Pb ages for granitoids from the Marivan pluton. Geochronometria 41, 207–215.

Shafaii Mogadam, H.S., Whitechurch, H., Monsef, I., Rahgoshay, M., 2009. Significance of Nain-Baft ophiolitic belt (Iran): Short-lived, transtensional Cretaceous back-arc oceanic basins over the Tethyan subduction zone. C.R. Geosci. 341, 1016–1028.

Shafaii Mogadam, H.S., Khedr, M.Z., Chiaradia, M., Stern, R.J., Bakhshizad, F., Arai, S., Ottley, C.J., Tamura, A., 2014. Supra-subduction zone magmatism of the Neyriz ophiolite, Iran: constraints from geochemistry and Sr-Nd-Pb isotopes. Int. Geol. Rev. 56, 1395–1412.

Shafaii Moghadam, H., Stern, R.J., 2011. Geodynamic evolution of Upper Cretaceous Zagros ophiolites: formation of oceanic lithosphere above a nascent subduction zone. Geol. Mag. 148, 762–801.

Shafaii Moghadam, H., Bröcker, M., Griffin, W.L., Li, X.-H., Chen, R.X., O'Reilly, S.Y., 2017. Subduction, high-P metamorphism, and collision fingerprints in South Iran: constraints from zircon U-Pb and mica Rb-Sr geochronology. Geochem. Geophys. Geosyst. 18, 306–332.

Shahbazi, H., Siebel, W., Pourmoafee, M., Ghorbani, M., Sepahi, A.A., Shang, C.K., Vousoughi Abedini, M., 2010. Geochemistry and U–Pb zircon geochronology of the Alvand plutonic complex in Sanandaj–Sirjan Zone (Iran): New evidence for Jurassic magmatism. J. Asian Earth Sci. 39, 668–683.

Shakerardakani, F., Neubauer, F., Masoudi, F., Mehrabi, B., Liu, X., Dong, Y., Mohajjel, M., Monfaredi, B., Friedl, G., 2015. Panafrican basement and Mesozoic gabbro in the Zagros orogenic belt in the Dorud–Azna region (NW Iran): Laser-ablation ICP–MS

zircon ages and geochemistry. Tectonophysics 647–648, 146–171.
Shand, S.J., 1943. The Eruptive Rocks, 2nd edn. John Wiley, New York (444p).
Sharland, P.R., Archer, R., Casey, D.M., Davies, R.B., Hall, S.H., Heward, A.P., Horbury, A.D., Simmons, M.D., 2001. Arabian plate sequence stratigraphy. GeoArabia 371 Special Publication 2, Bahrain, 3 enclosures.
Smirnov, V.A., Nelidov, V.P., 1962. Report on 1:200000 Prospecting Correlation of the Sylaimaniya-Choarta and Penjwin Area Carried Out in 1961. Unpublished Report, GEOSURV Lib., Baghdad, Report No 290. pp. 46.
Stacey, J.T., Kramers, J.D., 1975. Approximation of terrestrial lead isotope evolution by a two-stage model. Earth Planet. Sci. Lett. 26, 207–221.
Sun, S.S., McDonough, W.F., 1989. Chemical and isotopic systematic of oceanic basalts: implication for mantle composition and processes. In: In: Sunders, A.D., Norry, M.J. (Eds.), Magmatic in Oceanic Basins, vol. 42. Geological Society London, Special Publications, pp. 313–345.
Tanaka, T., Togashi, S., Kamioka, H., Amakawa, H., Kagami, H., Hamamoto, T., Yuhara, M., et al., 2000. JNdi-1: a neodymium isotopic reference in consistency with LaJolla neodymium. Chem. Geol. 168, 279–281.
Whalen, J.B., Currie, K.L., Chappell, B.W., 1987. A-type granites: geochemical characteristics, discrimination and petrogenesis. Contrib. Mineral. Petrol. 95, 407–419.